Selection of the Gridded Temperature Dataset for Assessment of Thermal Bioclimatic Environment Changes in Amu Darya River Basin

Obaidullah Salehie
Universiti Teknologi Malaysia
Tarmizi Ismail (tarmiziismail@utm.my)
Universiti Teknologi Malaysia
Shamsuddin Shahid
Universiti Teknologi Malaysia
Saad Sh Sammen
Kabul University
Anurag Malik
University of Diyala
Xiaojun Wang
Nanjing Hydraulic Research Institute

Research Article

Keywords: Gridded temperature data, bioclimatic indicators, trend analysis, Amu Darya, group decision-making, compromise programming, statistical metrics

Posted Date: July 26th, 2021

DOI: https://doi.org/10.21203/rs.3.rs-738934/v1

Selection of the Gridded Temperature Dataset for Assessment of Thermal Bioclimatic Environmental Changes in Amu Darya River Basin

Obaidullah Salehie[1,2], Tarmizi bin Ismail[1*], Shamsuddin Shahid[1], Saad Sh Sammen[2], Anurag Malik[3] and Xiaojun Wang[4,5]

[1]Faculty of Civil Engineering, Universiti Teknologi Malaysia, 81310 Johor Bahru, Johor, Malaysia

[2]Faculty of Environment, Kabul University, Kabul, Afghanistan

[3]Department of Civil Engineering, College of Engineering, University of Diyala, Diyala Governorate, Iraq

[3]Punjab Agricultural University, Regional Research Station, Bathinda-151001, Punjab, India

[4]State Key Laboratory of Hydrology–Water Resources and Hydraulic Engineering, Nanjing Hydraulic Research Institute, Nanjing 210029, China

[5]Research Center for Climate Change, Ministry of Water Resources, Nanjing 210029, China

* Corresponding author: tarmiziismail@utm.my

Selection of the Gridded Temperature Dataset for Assessment of Thermal Bioclimatic Environmental Changes in Amu Darya River Basin

Abstract

Assessment of the thermal bioclimatic environmental changes is important to understand ongoing climate change implications on agriculture, ecology, and human health. This is particularly important for the climatologically diverse transboundary Amy Darya River basin, a major source of water and livelihood for millions in Central Asia. However, the absence of longer period observed temperature data is a major obstacle for such analysis. This study employed a novel approach by integrating compromise programming (CP) and multicriteria group decision–making methods (MCGDM) to evaluate the efficiency of four global gridded temperature datasets based on observation data at 44 stations. The most reliable gridded data was used to assess the spatial distribution of global warming-induced unidirectional trends in thermal bioclimatic indicators (TBI) using a modified Mann-Kendall (MMK) test. Ranking of the products revealed Climate Prediction Center (CPC) temperature as most efficient in reconstruction observed temperature, followed by TerraClimate and Climate Research Unit (CRU). Assessment of TBI trends using CPC data revealed an increase in the minimum temperature in the coldest month over the whole basin at a rate of 0.03 to 0.08℃ per decade, except in the east. Besides, an increase in diurnal temperature range and isothermally increased in the east up to 0.2℃ and 0.6% per decade, respectively. The results revealed negative implications of thermal bioclimatic change on water, ecology, and public health in the eastern mountainous region and positive impacts on vegetation in the west and northwest.

Keywords: Gridded temperature data, bioclimatic indicators, trend analysis, Amu Darya, group decision-making, compromise programming, statistical metrics.

1. Introduction

Climatic variables, especially temperature and precipitation, control the phenology, productivity, abundance, interaction and geographical distribution of biodiversity and overall the function of biotic ecosystems. Organisms physiologically react differently to different thermal environments, which prefer homeothermy for adaptation (Błażejczyk, 2011). Environmental gradient and climate differences affect the germination and seedling process and plant populations' genetic structure (Hamasha et al., 2013). Therefore, the spatial distribution of species and biotic ecosystems depended on the different climatic characteristics. The bioclimate indicators are generally used to represent the climatic characteristics that affect the biotic system (Attorre et al., 2007; Miguet and Groleau, 2007; Noce et al., 2020; Schröder et al., 2014). Therefore, changes in bioclimatic indicators can indicate the impacts of global warming-induced climate change on living things (Pour et al., 2020). Climate change impacts on thermal bioclimatic are most certain and visible across the globe. Therefore, changes in thermal bioclimatic indicators (TBIs) and their implications have attracted more attention in recent years (Pour et al., 2020).

Many studies have been conducted to find how thermal bioclimate conditions affect the ecology. However, most of the recent studies were focused on the relations of bioclimatic condition in terms of temperature with human thermal comfort in urban areas where the effect of the urban island are dominant (Daemei et al., 2019; Gaitani et al., 2007; Kim et al., 2019; Ma et al., 2016; Meseguer-Ruiz et al., 2018; Sajani et al., 2008; Salat, 2007). Besides, few studies evaluated the implications of thermal bioclimate on crop growth and public health. For example, Moriondo et al. (2013) reported the possible consequence of future climate variability on the olive plants in the Mediterranean Basin. Fraga et al. (2019) showed climate change effect on rice bioclimatic growth conditions in Portugal. Recently, Bashir et al. (2020) showed an association of thermal climate with the spread of disease in New York. They found that temperature, among several other climatic variables, significantly correlate with the COVID-19 epidemic.

The Amu Darya is the most crucial transboundary river basin of Central Asia. Millions of people from five countries living in the basin depend on agriculture for their livelihood (Jalilov et al., 2016). The Amu Darya River basin (ADRB) hydrology has undergone a tremendous change in recent years due to human intervention in river flow. Climate change, particularly the rise in temperature, has worsened the situation. These caused severe damage to the ecology of the basin. The evaporation in the basin is high due to aridic climate conditions. The temperature rises caused an increase in evapotranspiration and water demand in the basin. The

changes in the thermal bioclimatic environment also influenced crop growth and yield. The changes in inter-annual and inter-seasonal temperature variability affected soil moisture and land suitability for cultivation. These changes severely affect agricultural productions, ecological services and livelihoods of agricultural dependent people (Sidike et al., 2016). Besides, public health is a growing concern due to changes in different TBIs related to human health. Evaluation of trends in TBIs of the ADRB basin is important for climate-resilient development planning of this most important river basin of Central Asia.

High spatial resolution and sufficient reliable temperature dataset are the major obstacles in assessing thermal bioclimate and its trends in the ADRB. Numbers of high-resolution gridded temperature data are available from different research organizations to substitute for observed data to assess climate (Bai et al., 2018; Guo et al., 2020; Saddique et al., 2020; Yasutomi et al., 2011; Yin et al., 2015). These datasets are generated from in-situ measurement, satellite retrieval, reanalysis, and a combination of satellite and observed data (Mahmood et al., 2019). These datasets can be used to assess thermal bioclimatic trends in the basin as an alternative to in-situ data. However, gridded datasets are usually associated with large uncertainties (Nijssen and Lettenmaier, 2004), originating from numerous factors, including interpolation from heterogeneous distributed gauge networks, measurement representativeness, and records errors (Newman et al., 2015). Therefore, it is required to evaluate their performance and reliability before using them for any purpose (Gampe and Ludwig, 2017; Musie et al., 2019).

Several studies evaluated the ability of gridded climate data in reconstructing local and global climate. General statistical metrics like correlation coefficient, mean bias and mean error are mostly used for this purpose (Ahmed et al., 2019; Colston et al., 2018; Xu et al., 2015). The major limitation of using the conventional metrics is the contradictory results provided by different metrics (Muhammad et al., 2019; Salman et al., 2018). Besides, artificial intelligence algorithms like random forest have been recently proposed to overcome the drawbacks of conventional statistics (Nashwan and Shahid, 2019). Likewise, different machine learning algorithms give different ranking outcomes for gridded climate products. The multicriteria group decision-making method (MCGDM) has been used to solve the aforementioned problem in recent years. The inconsistent results of various indices are combined in MCGDM to identify the best product (Salman et al., 2019).

Compromise programming (CP) is a class of multiple criteria decision-making methods known as the "distance-based" method. It is used to analyze multi-objective problems based on the concept of choosing a solution from a set of solutions considering the nearest to the

optimum points (Zeleny, 1973). Its strength over the conventional weighting approach is that it measures the minimum distance Pareto optimal point, especially when the distribution of the points is nonlinear (Zhang, 2003). CP was originally introduced by Zeleny (1973) and later used by many researchers related to their fields of studies, including analyzing hydrological and environmental issues (Brahim and Duckstein, 2011).

This study aims to (1) rank the best gridded temperature datasets in the ADRB through employing CP and group decision-making methods; (2) use the best gridded temperature dataset to assess the spatial distribution and trends in thermal bioclimatic indicators in ADRB to understand the possible consequences of global warming on agriculture and ecology in the basin. Four gridded temperature datasets were evaluated, namely the Climate Prediction Centre (CPC) global dataset, University of East Anglia Climatic Research Unit CRU TS V4.03 (CRU), Princeton University Global Meteorological Forcing dataset for land surface modelling (PGF) V3 and TerraClimate dataset. Trends in seven bioclimatic indicators related to the ecological environment of the basin are evaluated. The results presented in this study can be used for policy formulation to achieve sustainable development goals for the Central Asian nations. The identified best gridded temperature dataset can be used for climate change studies in the basin to overcome data scarcity challenges.

2. Study Area and Data

2.1 Amu Darya River basin

The Amu Darya river is the lengthiest transboundary river shared by five counties of Central Asia, including Afghanistan, Tajikistan, Kyrgyzstan, Turkmenistan and Uzbekistan (Jalilov et al., 2016; Schlüter et al., 2005), as shown in Figure 1. Rising from headwaters in the glacier and ice-packs in the mountains of Tajikistan, Kyrgyzstan and the north of Hindu Kush, it passes through Karakum and Kyzylkum deserts and drains into the Aral Sea (Kumar et al., 2019; Nezlin et al., 2004; Sun et al., 2019). The basin has a typical continental climate characterized by cold winter, hot summer, low precipitation, and relative humidity (Jalilov et al., 2013). The topography of ADRB ranges from 7,500 m in the upstream mountains to around 200 m in the downstream northwest plains with a delta and feeding the Aral Sea. The annual mean precipitation in ADRB is 464 mm. The maximum precipitation occurs upstream (Eastern Pamir) of the ADRB, nearly 2000 mm, while downstream receive a minimum, less than 100 mm/year. Precipitation mostly occurs in the form of snow in winter (Nov-May). The summer (Jun-Sept) is dry and hot with an average temperature of 35℃ which gradually decrease to 18℃

in the autumn and reaches to –8℃ to –20℃ in the winter (Gaybullaev and Chen, 2013; Wang et al., 2016).

Few attempts have been made earlier to estimate historical changes and future temperature projections in the basin using gridded temperature data, considering the scarcity of observed temperature data. Table 1 summarizes the major conclusions of those studies.

Table 1. Previous studies in the study area and nearby areas using gridded temperature data

Reference	Study Region	Data Used	Main Finding
White et al. (2014)	Amu Darya basin	CRU used as a reference for temperature projections	The temperature is projected to increase up to 5℃ by 2070–2099, which would cause a rise in irrigation needs by 10.6-16 %
Törnqvist (2013)	Amu Darya basin	Evaluation of CRU data in the basin	Large uncertainty in CRU temperature.
Lutz et al. (2013)	Amu and Syr River basins	PGMFD temperature	The temperature would increase nearly 2℃ between 2007 and 2050
Savoskul and Shevnina (2015)	Syr Darya basin	CRU temperature in GCM selection	CRU upscaled to match with GCM.
Shibuo et al. (2007)	Aral Sea catchment	CRU temperature for evaporation estimation	A rise in evaporation with temperature rise.
Sidike et al. (2016)	Amu Darya	PGMFD, WSD and CRUNCEP temperature	PGMFD simulated station data well.
Haag et al. (2019)	Central Asia	CRU temperature	CRU can replicate in-situ temperature patterns.
Khaydarov and Gerlitz (2019)	Uzbekistan	CHELSA temperature	CHELSA agreed with the observed temperature.
Wang et al. (2016)	Amu Darya basin	PGMFD temperature	Temperature rising between 0. and 0.3℃/decade, which would affect streamflow in the basin.

CRU=Climate Research Units; PGMFD=Princeton's Global Meteorological Forcing Data; CHELSA=Climatologies at high resolution for the earth's land surface areas; WSD= The one weather station dataset; CRUNCEP= The National Centers for Environmental Prediction (NCEP I and II) and Climatic Research Unit-NCEP.

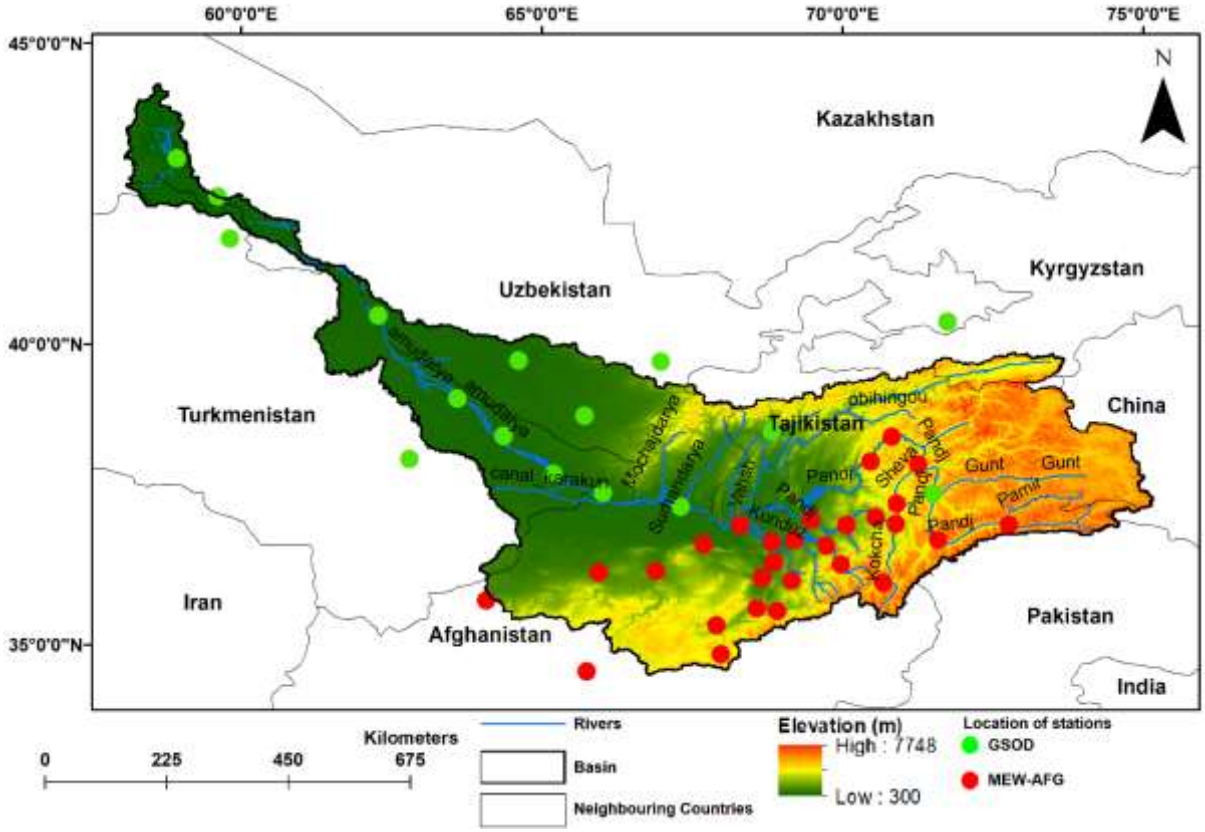

Figure 1. The geographical position of the Amu Darya River basin in Central Asia and the meteorological stations in the basin; the colour of the circles represents the data sources.

2.2 Observed temperature data

The observed monthly maximum and minimum surface temperature data were collected from the Ministry of Energy and Water of Afghanistan (MEW–AFG) and the website of Global Summary of the Day (GSOD): https://www7.ncdc.noaa.gov/CDO/cdoselect.cmd?datasetabbv=GSOD&countryabbv=&georegionabbv=. Data from the above-mentioned sources were collected for different stations, as shown in Figure 1. The data sources are represented using different colors. After screening the data, 44 stations with a longer period of data coverage were selected. The data were available for the period 1979 –2019. Also, few stations adjacent to the basin's boundary having a longer data availability period were considered. Stations having large missing data were not used in the current study. Most observations were located in the southeast, while relatively less in the west and southwest. Also, observation data were less in the northwest part of the basin. Overall, the station's distributions were more or less homogeneous over the basin.

2.3 Gridded temperature data

Four gridded temperature data that include National Oceanic and Atmospheric Administration (NOAA) Climate Prediction Center (CPC) global dataset, University of East Anglia Climatic Research Unit TS V4.03 (CRU), Princeton University Global meteorological Forcing dataset for land surface modelling V3 (PGF) and TerraClimate were evaluated as shown in Table 2. These data were obtained from the public domain in NetCDF format, which was subsequently extracted and analyzed using statistical software R. The gridded temperature products were evaluated according to their capability to reconstruct observed data for their common period 1979–2016.

Table 2. List of gridded temperature datasets with their spatiotemporal resolutions and availability periods.

Datasets	**Spatial resolution**	**Temporal resolution**	**Available Period**
CPC	0.5°	Daily	1979–2019
CRU V4.03	0.5°	Monthly	1901–2018
PGF	0.25°	Daily	1948–2016
TerraClimate	0.04°	Monthly	1958–2019

TerraClimate is a global gridded monthly climate dataset with 0.04° spatial resolution, available from 1958 to the present. TerraClimate, climatically interpolation for gridding the monthly station data obtained from the WorldClim dataset, coarse-resolution other monthly data productions of various climate variables (Abatzoglou et al., 2018). The TerraClimate data was downloaded from the site https://climatedataguide.ucar.edu/climate–data/terraclimate–global–high–resolution–gridded–temperature–precipitation–and–other–water. The CPC is a station observation-based product, generated at the Climate Prediction Center, National Centers for Environmental Prediction (Tanarhte et al., 2012; Xie et al., 2010). The data are available at ftp://ftp.cdc.noaa.gov/Datasets/cpc_global_precip/. The CRU used angular distance weighting interpolation for gridding the monthly station data obtained from different international and national organizations covering the global land except for Antarctica (New et al., 2000). The data was downloaded from https://crudata.uea.ac.uk/cru/data/hrg/cru_ts_4.03/. Princeton University has developed the PGF datasets by combining several global observation-based datasets with the National Centers for Environmental Prediction–National Center for

Atmospheric Research (NCEP–NCAR) reanalysis (Sheffield et al., 2006). It was downloaded from http://hydrology.princeton.edu/data/pgf/v3/0.25deg/daily/.

3. Research Method

3.1 Procedure

The procedure used to rank gridded temperature datasets and analyze TBI trends is shown using a flowchart in Figure 2. Homogeneity of station data was first evaluated and then compared with the gridded data. The assessment of gridded data is generally done either by interpolation gridded data at observed locations or correlation with nearby stations (Caesar et al., 2006). In the present study, gridded temperature data were interpolated at the observation location using the inverse distance weighting (IDW) method for comparison. The results obtained using different statistical metrics were summarized using CP for the ranking of the products.

The maximum (Tmx) and minimum (Tmn) temperature data of the best gridded product were used to estimate the annual time series of the TBIs at each grid location. The Sen's slope was employed to calculate the change in TBIs, and the modified Mann-Kendall (MMK) test was used to assess the statistical significance in change. The methods employed in this study are explained below.

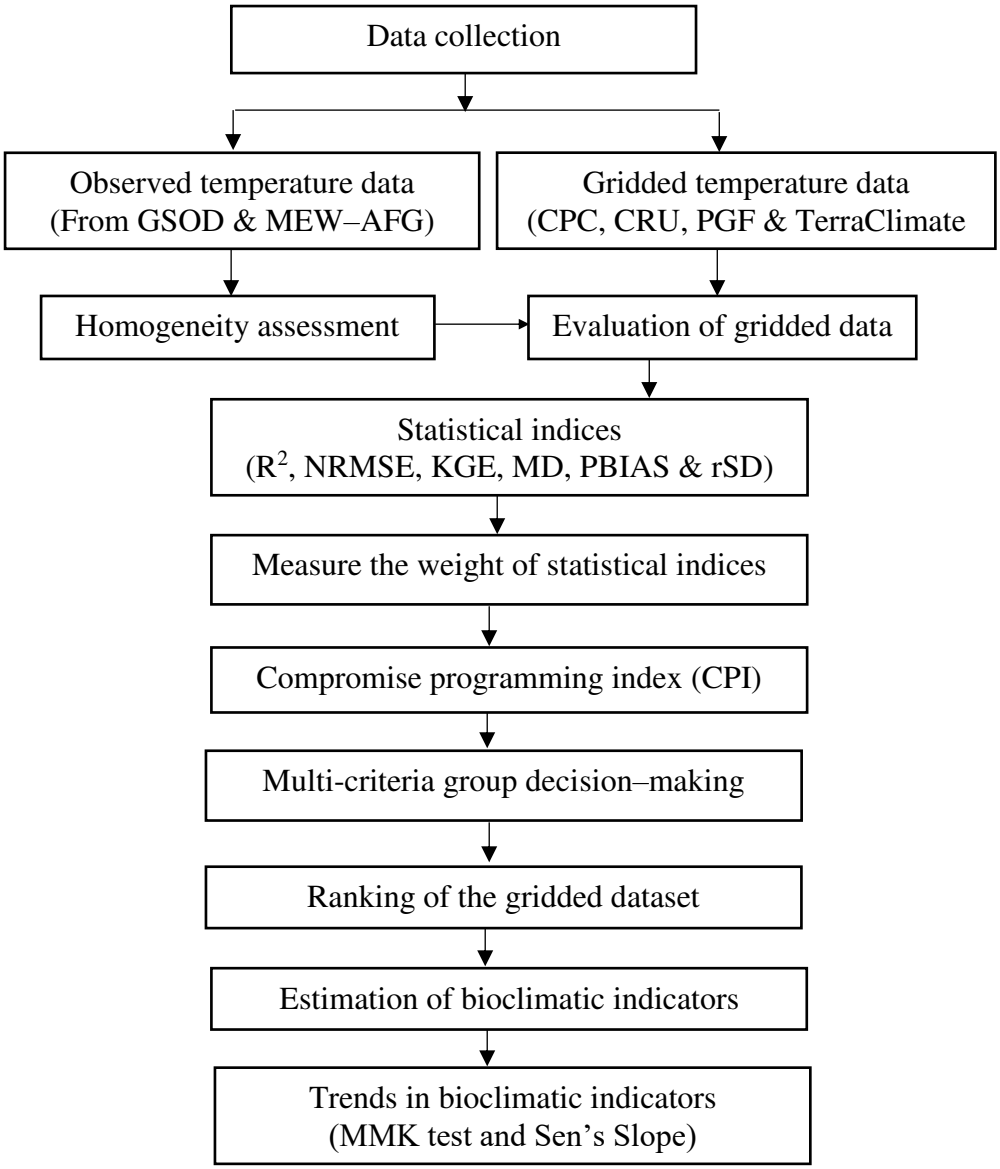

Figure 2. The general methodology of the current study

3.2 Performance evaluation

Six statistical indices including the coefficient of determination (R^2), normalized root mean square error (NRMSE), percentage of bias (PBIAS), Kling–Gupta Efficiency (KGE), modified index of agreement (MD), and the ratio of standard deviation (rSD) were employed to assess the accuracy of temperature products. These statistics can evaluate the performance of different properties of in-situ temperature like the average, variability and pattern. Table 3 shows the expression, possible range and ideal values of the metrics.

Table 3. The statistical indices used for the assessment of gridded temperature data

Index	Range	Optimal Value
$R^2 = \left(\frac{\sum_{n=1}^{n}(x_o - \bar{x}_o)(x_g - \bar{x}_g)}{\sqrt{\sum_{n=1}^{n}(x_o - \bar{x}_o)^2 \sum_{n=1}^{n}(x_g - \bar{x}_g)^2}} \right)^2$	– 1 to 1	1
$NRMSE = \frac{\left[\left(\frac{1}{n}\right)\sum_{i=1}^{n}(x_g - x_o)^2\right]^{1/2}}{sdv(x_o)}$	0 to ∞	0
$PBias = \left(\frac{\sum_{i=1}^{N}(x_o - x_g)}{\sum_{i=1}^{N} x_o} \right)$	– ∞ to ∞	0
$KGE = 1 - \sqrt{(r-1)^2 + (\beta - 1)^2 + (\gamma - 1)^2}$ $\beta = \frac{\mu_g}{\mu_o} \quad and \quad \gamma = \frac{\sigma_g/\mu_g}{\sigma_o/\mu_o}$	– ∞ to 1	1
$MD = 1 - \frac{\sum_{i=1}^{n}(x_o - x_g)^j}{\sum_{i=1}^{n}(\lvert x_g - \bar{x}_o \rvert + \lvert x_o - \bar{x}_g \rvert)^j}$	0 to 1	1
$rSD = \frac{sd(x_o)}{sd(x_g)}$	– ∞ to ∞	1

where X_g and X_o are the gridded (g) and observed (o) temperature respectively; r is Pearson's correlation; β represents the bias; γ is a fraction of the coefficient of variation. μ and σ are the data mean and standard deviation.

3.3 Compromise programming (CP)

The present study used CP to merge the outcomes obtained using different statistical indices to derive a single metric. The CP identifies the best product by estimating its lowest distance from the ideal point (Raju et al., 2017; Zeleny, 1973). The compromise programming index (CPI) is presented as,

$$\mathrm{CPI} = \left[\sum_{\mathrm{i}=1}^{\mathrm{n}} \left| \mathrm{x}_{\mathrm{i}}^{1} - \mathrm{x}_{\mathrm{i}}^{*} \right|^{\mathrm{p}}\right]^{1/\mathrm{p}} \qquad (1)$$

Where i is the statistical index; x_i^1 is the normalized value of index i for gridded dataset 1; x_i^* is the normalized ideal value of index i; and p is the parameter (p-value 1 is for linear and 2 for measuring squared Euclidean distance). In the current research, the p-value is considered 1 for the linear measure. CPI can be any positive value, but the smaller CPI of a gridded temperature indicates its closeness to observed temperature data.

CP can rank different data products at a station location. But the challenge remains in deciding about the best product for the whole basin, based on ranking at different stations. A multicriteria group decision–making method (MCGDM) method was used to order the data

products based on their performance. In the proposed method, each gridded product was weighted according to the rank obtained by the product at different observation points. The weight to a product is provided as the reverse of the rank, which means if a product obtained 1st, 2nd and 3rd rank at r_1, r_2 and r_3 stations, its integrated index, I_x is calculated as

$$I_x = r_1(1/1) + r_2(1/2) + r_3(1/3) \quad (2)$$

3.4 Thermal bioclimatic indicators

The spatiotemporal changes in 7 TBIs were evaluated in this study. The details of the TBIs are summarised in Table 1.

Table 1. Description of thermal bioclimatic indicators evaluated in this study

Index	Estimated method	Unit
TBI1	The yearly mean of daily average temperature	0℃
TBI2	The yearly mean of daily temperature ranges	0℃
TBI3	Temperature variation between hot and cold seasons	%
TBI4	The standard deviation (SD) of monthly average temperature in a year	0℃
TBI5	The maximum temperature in the hottest month	0℃
TBI6	The minimum temperature in the coldest month	0℃
TBI7	The monthly temperature range of a year	0℃

3.5 Trend analysis

Sen's slope is a nonparametric method that estimates the change over time from time series data (Sen, 1968). It estimates the change as the median of all slopes calculated for two successive data points.

Man-Kendall (MK) is a nonparametric test used for non-normally distributed data (Kendall, 1975; Mann, 1945). It provides two measures, significant level and sign; the farmer shows the strength while the latter indicates the direction of change. Hamed (2008) improved the MK test to remove the impacts of long-term persistence in data series on-trend significance. This allows unidirectional trend evaluation due to global warming. The modified MK (MMK) test procedure begins with assessing the trend using the MK test. If there is a significant trend in the time series, the MMK test de-trends the series and estimates the Hurst coefficient. This estimate of the secular trend due to global warming by omitting the trends that arise from

natural climate fluctuation. Different recently published articles provide details of the MMK test (Nashwan et al., 2019; Khan et al., 2019).

4. Results

4.1 Performance assessment of gridded maximum temperature

4.1.1 Mean daily maximum temperature

Figure 3 shows the geographical distributions of observed and estimated Tmx over ADRB. Observed Tmx at 44 locations for the period between 1979–2016 were interpolated at 0.5° resolution using the IDW method to generate the map. The results showed that all the gridded datasets provided an almost similar spatial pattern of observed Tmx over the basin. Overall, the center and western part of the basin showed a higher temperature (~ 33℃), while the basin's east showed a lower temperature (nearly −15℃).

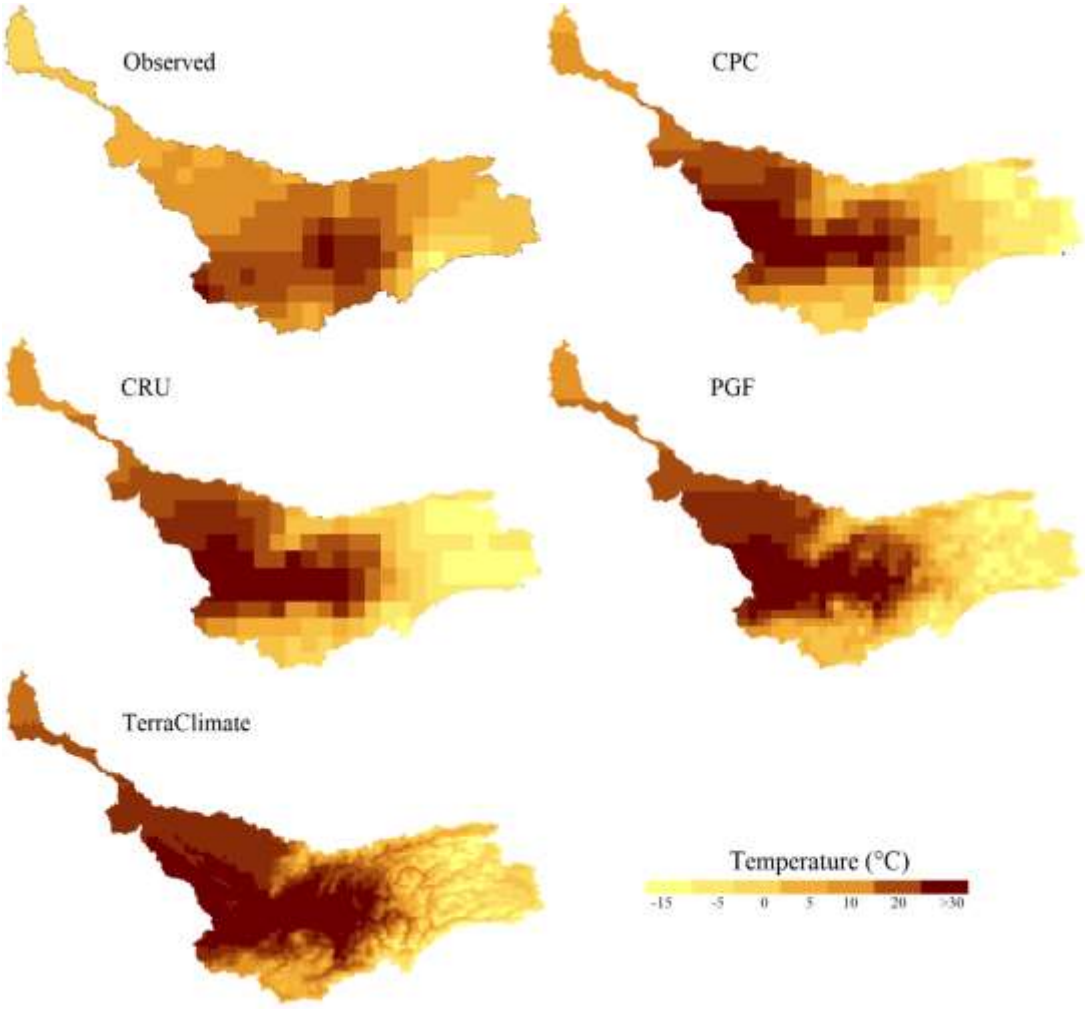

Figure 3. Annual average of daily maximum temperature estimated by different gridded datasets over the basin for the available periods.

4.1.2 Statistical evaluation of maximum temperature

The metrics, R^2, KGE, MD, rSD, PBIAS and NRMSE, were computed at all the station locations for all the gridded data to assess their capability in reconstructing observed Tmx. Figure 4 presents the results obtained for different data products at all locations using box plots. The highest median of R^2 was observed for CRU followed by CPC, PGF and TerraClimate. The KGE for all the products at all the locations was negatively skewed. The TerraClimate received the highest value of KGE. The median of MD was higher for CPC while more or less the same for the other products. The median of rSD was nearest to its ideal value was for CPC, followed by TerraClimate, CRU and PGF. The CPC showed the lowest bias (PBIAS) and NRMSE.

Table 4 shows the ranking of the products in replicating Tmx in terms of six statistical metrics. The values in the table indicate the number of stations at which a product ranked first in terms of a particular metric. The results showed the best performance of CRU in R^2 at most of the locations (28), followed by CPC (25) and PGF (12). More than one product received the same R^2 at some stations and thus, obtained the same rank. For example, CRU and CPC obtained the highest R^2 value (1) at locations (lat, long), (39.083, 63.6), (40.467, 62.283), (41.75, 59.817) and (37.833, 65.2). Therefore, both were ranked 1st at those locations. It made the total number of stations where different products received the highest rank more than the total station number (44).

In terms of KGE, TerraClimate was the best at 18 stations, followed by CPC. The TerraClimate achieved the best rank at most stations in rSD (23) and NRMSE (23). The CPC was best in MD at most stations (30) and CRU for PBAS (15). The results indicate contradictory outcomes based on different metrics. Therefore, CP was employed to merge the outcomes of all metrics to have a common index (CPI) for ranking.

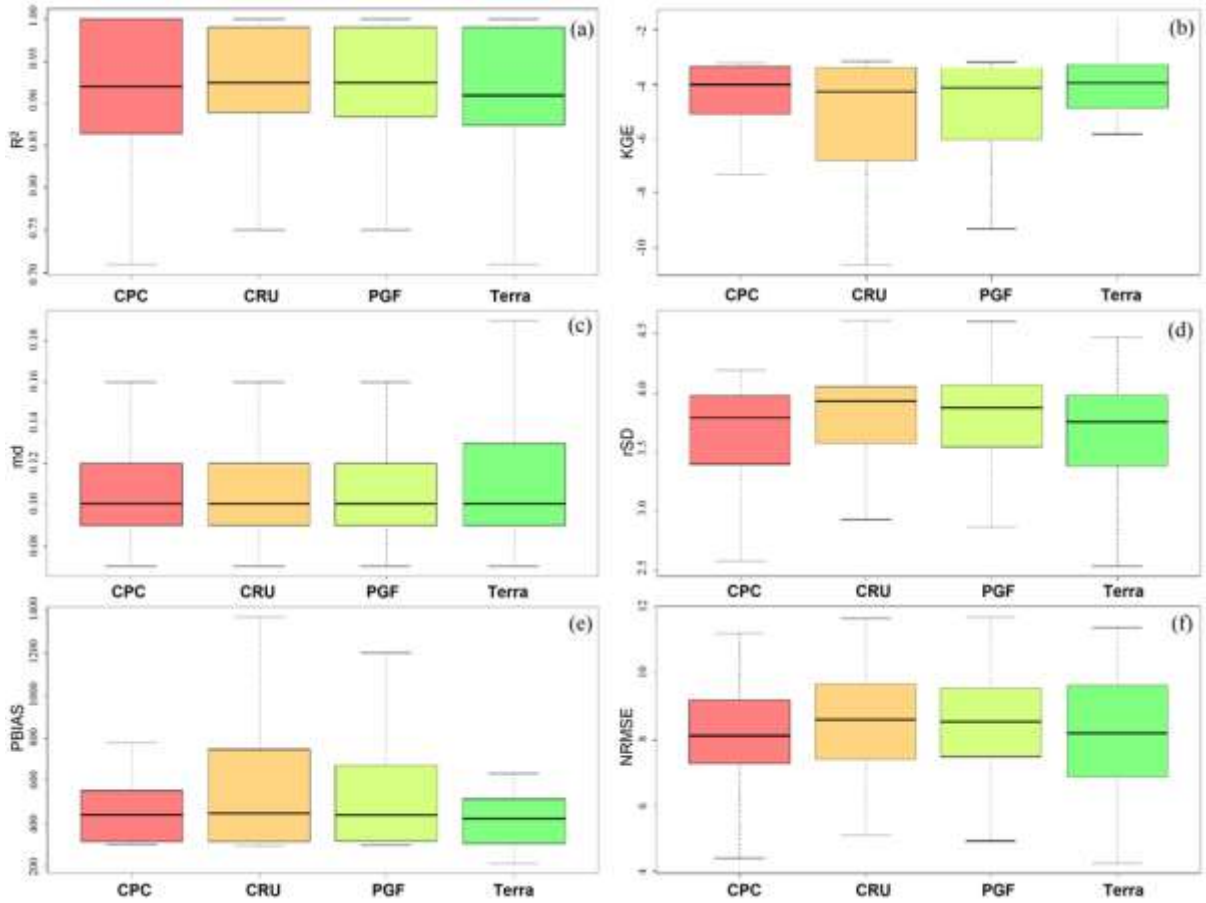

Figure 4. Boxplot shows different gridded dataset's performances in replicating maximum temperature at different locations based on the statistical metrics.

Table 4. The number of observation locations at which different gridded datasets received the higher rank in terms of different statistical metrics.

Gridded maximum temperature dataset				
Statistical metrics	CPC	CRU	PGF	Terra
R^2	25	28	20	12
KGE	14	7	6	18
MD	30	19	21	29
rSD	18	1	2	23
PBIAS	10	15	5	14
NRMSE	18	1	2	23

4.1.3 Ranking of gridded maximum temperature datasets

Figure 5 shows the CPI estimated for different gridded Tmx datasets at 44 stations using a heatmap. A lower value of CPI represents good performance, and therefore, the red color in the heatmap indicates higher capability. Similarly, the green color represents less capability. Figure 5 reflects many cells with colors ranging from deep red to yellow for CPC, followed by TerraClimate, PGF and CRU.

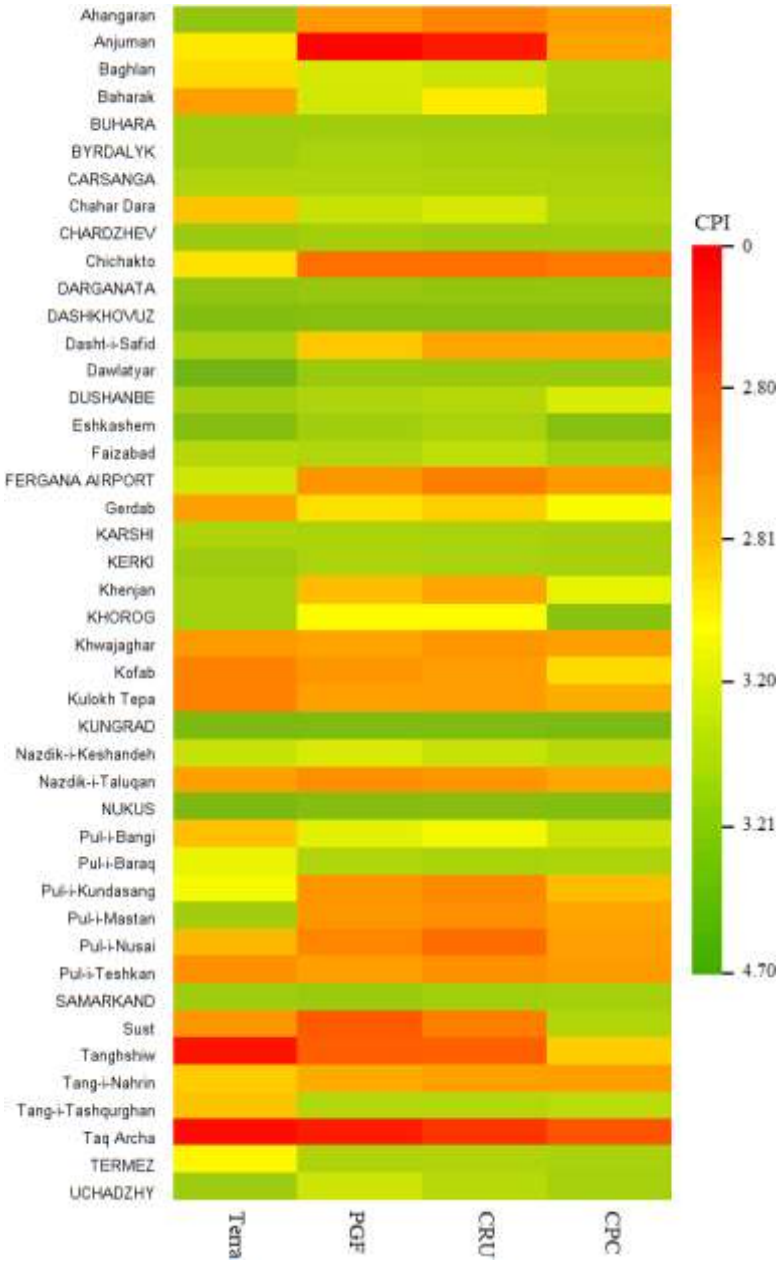

Figure 5. Heatmap of CPI for all gridded maximum temperature datasets used in this study

4.2 Performance assessment of gridded minimum temperature

A similar analysis was conducted for Tmn. The spatial distribution of Tmn over the basin for 1979–2016, estimated using the station and gridded data, is given in Figure S-1. Like Tmx, the higher value of Tmn was in the center and west part, and the lowest temperature was in the east part of the basin. TerraClimate showed the lowest estimation of Tmn (–24.48℃) followed by PGF (–14.78℃), CRU (–12.84℃) and CPC (–7.73℃). Figures S-2 presents the performance of the gridded data in replicating observed Tmn at different stations based on CPI (heatmaps). The figure indicates the better performance of CPC in most of the stations.

4.3 Group decision-making process of maximum and minimum temperature

The MCGDM was used to merge the ranks of the gridded data products at different stations to select the best product for the entire basin rationally. Table 5 presents the ranks for Tmx and Tmn datasets obtained using CPI and the ranks obtained by merging them using MCGDM. The data products were assigned a weight based on the number of stations they were ranked 1st, 2nd and 3rd. Finally, an integrated MCGDM index was estimated using equation (2). The higher value of the index indicates a better performance of a product. The overall ranking using MCGDM revealed CPC as the best temperature product in the basin, followed by TerraClimate and PGF.

Table 5. The overall ranking of the gridded maximum and minimum temperature datasets in the Amu Darya River basin, based on multicriteria group decision analysis.

Product	Station Rank (Max Temp)			Station Rank (Min Temp)			MCGDM Index
	1st	2nd	3rd	1st	2nd	3rd	
CPC	19	17	5	18	5	8	9.9
CRU	2	9	20	10	13	14	4.4
PGF	3	12	15	6	17	18	4.7
Terra	20	6	4	10	9	4	7.9

4.4 Spatial analysis of the trends in thermal bioclimate indicators

The estimated trends in the TBIs at 241 CPC grids locations were used to generate maps and assess the geographical distribution of their trends over the ADRB. A similar legend was applied to present the value of change in all bioclimate indicators except TBI3 (different unit)

to compare the changes among different indicators easily. The color ramp of the maps indicates the changes estimated by Sen's slope. The red indicates a positive, while the green indicates a negative change. The black dot placed in the center of each box specifies the trend significance obtained using MMK test at a 95% confidence interval.

4.4.1 Annual average temperature (TBI1)

The TBI1 indicates the average thermal condition in the basin. It gives information about approximate total energy inputs received in the basin for an ecosystem. Figure 6a, represents the geographical variability of TBI1, and Figure 6b shows the trends in TBI1 in the ADRB. The TBI1 over the basin ranges from –2℃ to 18.8℃. The maximum TBI1 is in the center and the minimum in the east of the basin. Figure 1b reveals a significant reduction in TBI1 in the north-western and central parts of the basin. Despite a rising tendency in the TBI1 in the eastern part of the basin, the increases are still not significant. In general, a reduction in average temperature in the high-temperature zone and increasing tendency in the cold region indicates a more homogeneous temperature distribution in the basin in recent years.

TBI1 is directly related to vegetation health and the species richness of an area. Islam et al. (2021) showed positive relation of TBI1 with NDVI of Bangladesh. Adhikari et al. (2018) showed that TBI1 determines the species richness in the mountainous region of South Korea. Sosa and Loera (2017) found the highest positive correlation of TBI1 with species richness in Mesoamerica among all other indicators. Käfer et al. (2020) assessed the thermal limits of European Seed Bugs, critical to thermal maxima (mean=45.3℃) and showed their high correlation with TBI1 and TBI5. The decrease in TBI1 over a major region of ADRB can have severe negative implications on vegetation and ecology in the basin.

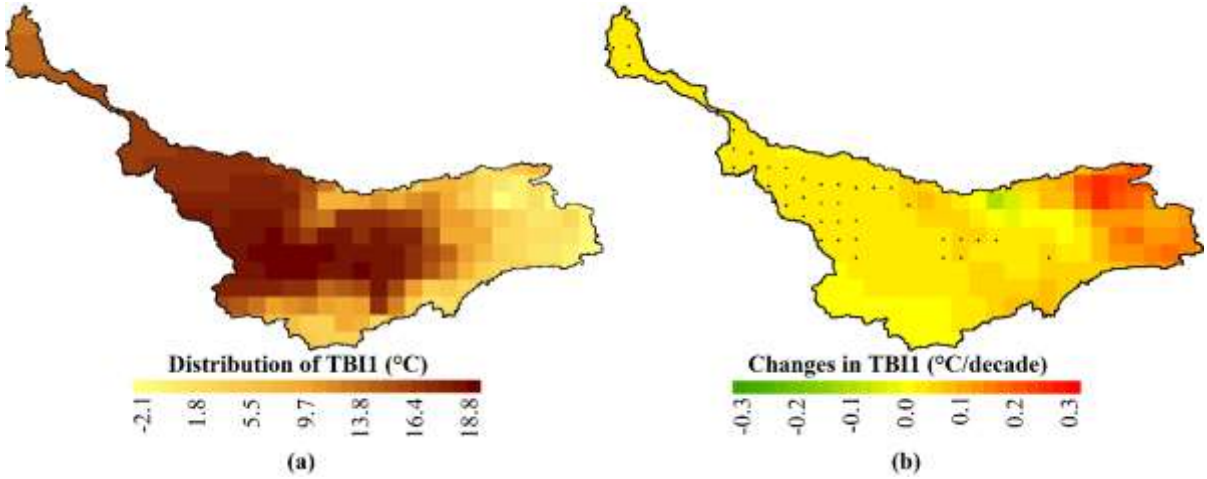

Figure 6. (a) Spatial pattern of yearly average temperature (TBI1); (b) trends in TBI1 (℃/decade) in the study area.

4.4.2 Diurnal tem Gridded temperature data, bioclimatic indicators, trend analysis, Amu Darya, group decision-making, compromise programming, statistical metrics *perature range (TBI2)*

This *TBI2* indicates the daily fluctuation of temperature or the differences in daily Tmx and Tmn. Therefore, TBI2 indicates the relative change in maximum and minimum temperature. Figure 7(a and b) show the spatial distribution of TBI2 and its trend over ADRB. The TBI2 is higher in the high-temperature region in the west and less in the cold region in the east. The TBI2 trends revealed a significant rise in the cold eastern zone. The increases were more than 0.17℃/decade in some locations. A faster rise in Tmx than Tmn in the cold region caused a sharp increase in TBI2.

The TBI2 defines the relative difference in maximum and minimum temperature and is often used to show global warming-induced climate change (Noce et al., 2020; Shahid et al., 2012). Increases in TBI2 can significantly affect the vegetation and public health of a region. Evans and Lyons (2013) found an increase in the TBI2 caused forest death in the east of Perth in Western Australia. Yaro et al. (2021) found TBI2 has significant impacts on the geospatial distribution of soil-transmitted helminths (STHs). TBI2 is positively related to mortality, especially from heart and respiratory-related diseases (Cheng et al., 2014). Therefore, increases in TBI2 in the east of the basin can severely affect the region's vegetation, soil, and public health. The TBI2 is generally negatively related to the precipitation of a region (He et al., 2015).

The increase in TBI2 can reduce precipitation over the eastern mountainous zone, which is the basin's water supply source. This can severely affect the water availability in the basin.

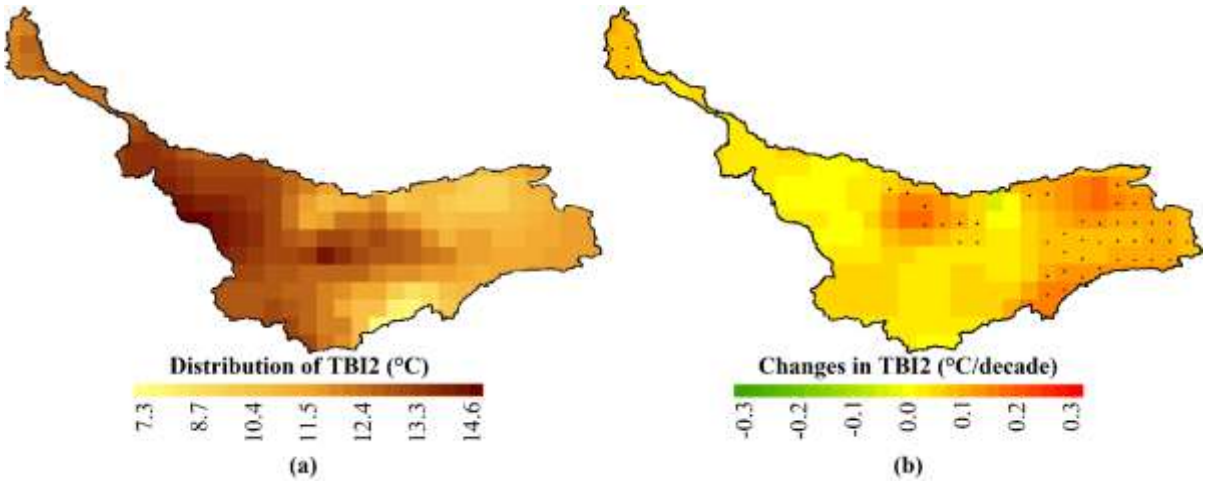

Figure 7. (a) Spatial distribution of diurnal range (TBI2); (b) trends in TBI2 (℃/decade) in the basin.

4.4.3 Isothermality (TBI3)

TBI3 is the ratio of the diurnal temperature range (DTR) or TBI2 to seasonal temperature fluctuation expressed as a percentage. Figure 8a shows that TBI3 in ADRB varies from 31.5 to 54.3%, with higher variability in the center, south and western part of the basin. Results of the trend analysis showed a steady rise in TBI3 in the basin's east (Figure 8b). A large increase in TBI2 in the east of the basin was the cause of a significant rise in TBI3.

The species distribution of an area depends on the temperature fluctuation of the area within a year (Nix, 1986; O'donnell and Ignizio, 2012). Therefore, isothermality plays a vital role in the biodiversity and ecology of a region. Rai et al. (2016) reported the most significant effect of TBI3 on the plant composition among all the indicators. Sommer et al. (2010) estimated a reduction of biological diversity with an increase in temperature. Reitalu et al. (2014) also found an inverse relationship of species richness, particularly grasslands with TBI3. Other studies also showed negative consequences of increasing TBI3 on forest and bird species (Distler et al., 2015; Zhang et al., 2013). The TBI3 showed a significant rise in the east and

central-north of the basin. Increasing TBI3 would negatively affect mountain forests and mountain ecology in those mountainous regions significantly.

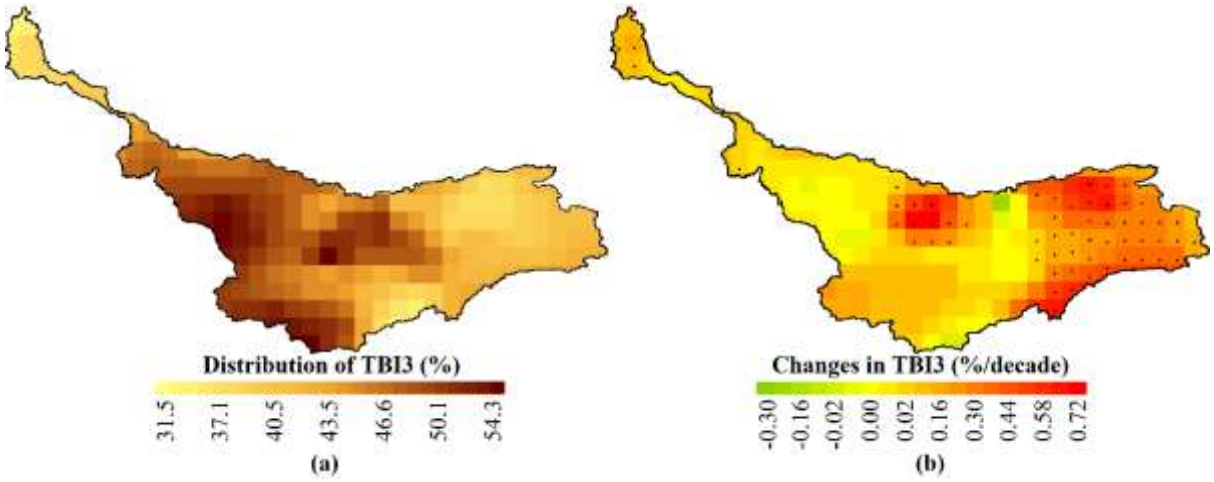

Figure 8. (a) Geographical distribution of isothermally (TBI3); (b) trends in TBI3 (%/decade) in the basin.

4.4.4 Temperature seasonality (TBI4)

TBI4 estimates the SD of the monthly mean temperature over a year, and thus, temperature variability within a year. The larger SD shows more variability of temperature in a region (Noce et al., 2020). Therefore, higher TBI4 indicates both hot and cold extremes in a region. The TBI4 in the study area (Figure 9a) ranges from 7.4 to 11.5℃. It is maximum in the northwest, where the temperature is predominantly high. Besides, it is high in the cold eastern region. The MMK test showed the TBI4 changes in the basin are insignificant (Figure 9b). However, there was a rising tendency in TBI4 in the east of the basin.

Generally, people experience higher thermoregulatory stress in a high TBI4 region (Monterroso et al., 2014). Wang et al. (2017) found that TBI4 and annual rainfall (TBI12) as the major drivers of coniferous forest coverage across China. A small change in TBI4 strongly affects the distribution of many species. Besides, the increase in temperature seasonality may increase temperature-related risks (Hadi Pour et al., 2019). Mancinelli et al. (2019) showed the direct association of thermal seasonality with non-arboreal foliage coverage. The rises in TBI4 can affect public health and vegetation in the southeast of the basin.

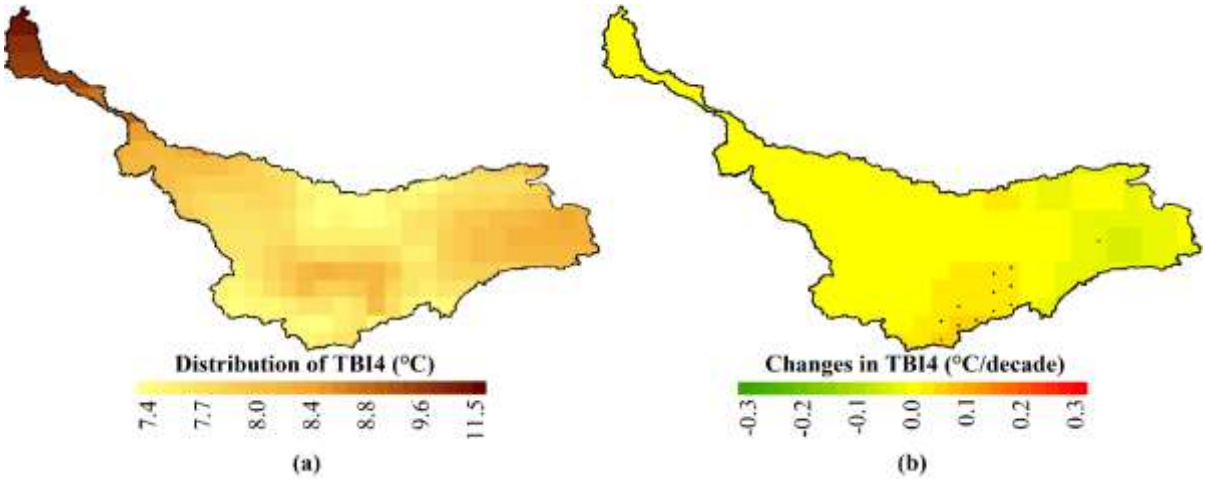

Figure 9. (a) Geographical variability; and (b) trends in temperature seasonality (℃/decade) in the basin.

4.4.5 Maximum temperature of warmest month (TBI5)

TBI5 provides an understanding of the effect of warm temperature anomalies over the year, which greatly influences species distribution. The TBI5 in the basin ranges from 16.5 to 40.1℃ (Figure 10a). The higher values of TBI5 were in the center, west and northwest of the basin. It indicates a higher susceptibility to the region of heat extremes. The MMK test revealed an increase in TBI5 in the center part of the basin by up to 0.3℃/decade (Figure 10b). It indicates increasing TBI5 in the region where it is already high. The increasing TBI5 in the region with high summer temperatures has increased the vulnerability of hot extremes like heatwaves in the region. This increase in TBI5 would also increase the discomfort to the residents of this aridic region, reduce water availability through the increase of evaporation and decline agricultural productivity.

Reitalu et al. (2014) showed that the TBI5 is negatively associated with phylogenetic diversity within the Baltic Sea region. Therefore, a rise in TBI5 in central ADRB may disturb the thermotolerant level of many species, spread diseases and cause other environmental effects (Hadi Pour et al., 2019).

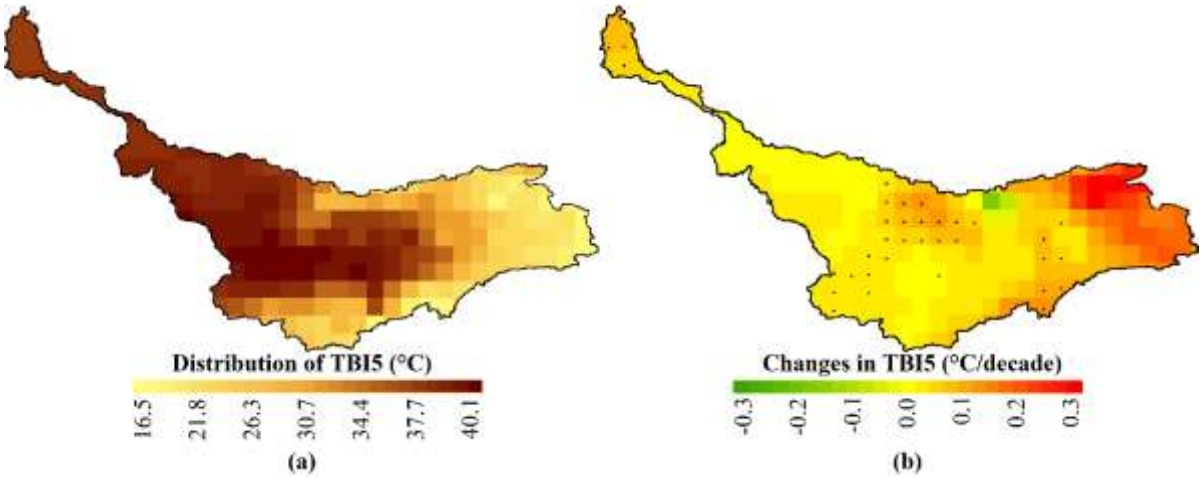

Figure 10. (a) Spatial distribution of maximum temperature of the warmest month (TBI5); (b) trends in TBI5 (℃/decade) in the basin.

4.4.6 Minimum temperature of coldest month (TBI6)

TBI6 measures Tmn in the coldest month, and therefore, it provides an understanding of susceptibility to clod extremes. The Tmn in the coldest month is below zero in most of the basin (Figure 11a). The Tmn is less than –20℃ in the eastern mountainous region and nearly zero in the central region, where summer maximum temperature goes as high as 40℃. The MMK test revealed a rise in TBI6 over the whole basin, except in the west (Figure 11b). Increases in TBI6 is most of the basin indicates a gradual reduction of clod extreme in most region. However, the TBI6 is not changing in the east, where it is lowest. This means cold wave vulnerability remains in the high susceptible region of the basin. Besides, the increase in Tmn in the coldest month over a large region of the basin might affect the population of coniferous plants in the tundra, which prolific more in a frost environment (Li et al., 2016). It can also increase species distribution in the west and northwest of the basin, where TBI6 was increasing fast (Ancillotto et al., 2016; Koo et al., 2015).

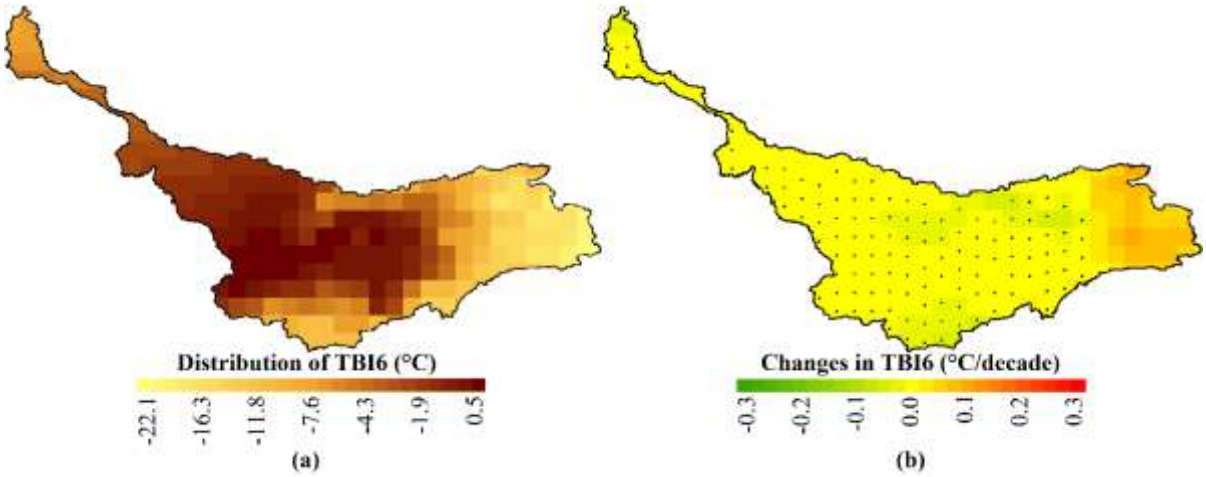

Figure 11. (a) Spatial distribution of minimum temperature of the coldest month (TBI6); (b) trends in TB6 (℃/decade) in the basin.

4.4.7 Temperature annual range (TBI7)

TBI7 is the difference in Tmn of the coolest month and Tmx of the hottest month. Therefore, it provides an understanding of temperature anomalies over a year. This information helps to know the impact of extreme temperature conditions on biodiversity. Figure 12a presents the geographical variability of TBI7 in the basin. The highest TBI7 was in the northwest (> 32℃) and lowest in the central region (< 25℃). The large values of TBI7 in the northwest indicate the area's susceptibility to both hot and cold extremes. The MMK test showed an increase in TBI7 only over a small area in the center north at a rate of nearly 0.1℃/decade (Figure 12b). The increase in TBI7 was mostly in the region where it is less. This indicates the susceptibility of both hot and cold extremes in the less susceptible region is increasing. The increase in TBI7 in the central-south region of the basin can have some other implications. Dakhil et al. (2019) reported a greater influence of TBI7 on coniferous forests distribution than precipitation in Tibetan Plateau China. Hradilová et al. (2019) showed significant relation of TBI7 to germination responsivity of pea seed. Yaro et al. (2021) significant relationship of TB7 with the geospatial variability of soil helminths (STHs) in Kogi East, North Central Nigeria.

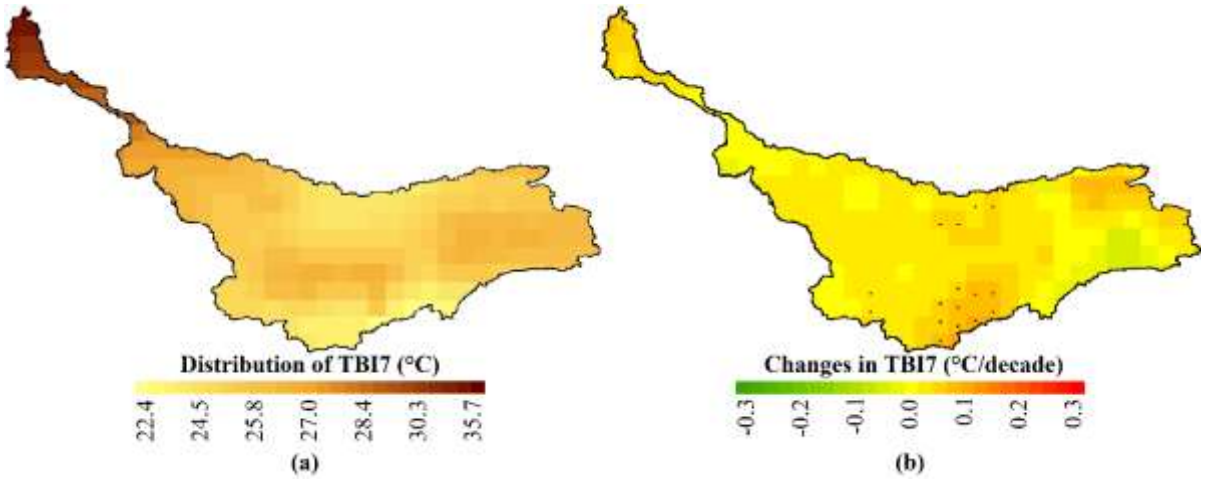

Figure 12. (a) Spatial distribution of the difference in minimum temperature of the coolest month and maximum temperature of the hottest month (TBI7); (b) trends in TBI7 (°C/decade) in the basin.

5. Discussion

The performance of four widely used gridded temperature datasets was assessed in this study. The objective was to find the most appropriate product for temperature analysis in the ADRB, where scarcity of in-situ data is the major barrier for climatological studies. The CP was employed to evaluate the ability of gridded temperature products. The CP is a multicriteria decision-making method known as the "distance-based" method, which solves multi-objective problems by measuring the distance of a solution closer to the ideal point. It is less computationally intensive and avoids decision makers' choices (Gan et al., 1996). The major strength of CP is to find the real Pareto optimum curve when the optimal points are heterogeneously distributed, a task that the conventional weighting methods are failed to do (Zhang, 2003). Statistical measures fail when the gridded data over- and underestimate in-situ data simultaneously. Therefore, GP overcomes these problems by combining the overall performance of a gridded dataset by comparing the statistically obtained outcomes (Behar et al., 2015; Fan et al., 2018; Jamil et al., 2020). Also, the statistical measure cannot rank and compare numerous models in such a way as to select the best. Still, GP does it easily and accurately by using all measures (Despotovic et al., 2015). Therefore, it is expected that the ranking of gridded temperature obtained using CP is robust.

The present study identified CPC as the most suitable product for replicating both maximum and minimum temperatures. Literature review suggests limited studies in the basin to evaluate the ability of gridded temperature products (Haag et al., 2019; Sidike et al., 2016;

White et al., 2014). Therefore, it was not possible to make a critical comparison with previous findings. However, the findings of those few existing studies collaborate with the results presented in this article. White et al. (2014) used CRU for the ADRB and showed that the product is not fair to provide good climatic input for water assessment. The present study also showed relatively poor performance of CRU data. Sidike et al. (2016) used Tmx and Tmn of PGF, WSD and CRUNCEP datasets for hydrological simulations in ADRB. They found that PGF simulated the observed data well, although underestimated high and overestimated low temperature. Haag et al. (2019) used CRU data to assess temperature changes in central Asia. Their results showed a good correlation of CRU data with available observed data. However, Sidike et al. (2016) and Haag et al. (2019) did not evaluate the ability of CRU and PGF with other gridded temperature datasets used in this study. The present study revealed that though CRU and PGF showed good correlations with observed temperature, their performance is poorer than CPC in ADRB.

Several previous studies used different gridded temperature datasets to evaluate temperature changes in the ADRB. Wang et al. (2016) used PGF temperature data to assess temperature trends in ADRB. They showed a rise in average Tmx and Tmn by 0.2 and 0.3℃/decade at a 99 % confidence interval. It indicates a rise in daily mean temperature in ADRB. The present studies also showed a rise in the average temperature over most of the basin. Haag et al. (2019) used CRU data and showed a rise in annual mean temperature by 0.28℃/decade at a 95% confidence level. They also showed that the plain area has a relatively higher temperature trend compare to mountains areas. It is also consistent with the results presented in this study. The present study showed an increase in average temperature in the central plain land and no significant change in the eastern mountainous region.

The results discussed above indicate similar estimates of spatiotemporal variability of temperature trends in ADRB using CPC, the best product and CRU, the least performing product. However, the spatial coverage of the trends estimated using CPC data was different from the earlier studies. The trend significance was also much less in this study than in the previous studies. This is because of the usage of CPC data and the MMK test. Nashwan, Shahid and Wang (2019) estimated the relative capability of different gridded rainfall products for trend analysis in Bangladesh. They showed rainfall trends significantly vary for different gridded data products. Therefore, they suggested evaluating the relative performance of different gridded data products to find the best product before their use for trend analysis. Therefore, the difference in spatial coverage of trends between CPC in the present study and CRU in the earlier studies is due to the quality of gridded temperature data. The present study

suggests that temperature studies in ADRB should be conducted using CPC data for better reliability.

The MMK test rather than MK test was employed in this study for evaluation of change significance. The trends in climate series may occur due to existing multi-year cycles in temperature series. Such cycles arise due to the influence of different atmospheric oscillations like the Mediterranean oscillation. The length of the cycles varies widely, with some are higher than 50 years (Khan et al., 2019). The MK test shows significant trends, often due to variability in data series because of these embedded cycles. The MMK test can avoid this and provides unidirectional trends. Therefore, the trend detected in this study is much less than that detected in previous studies. The trends presented in this study is due to climate variability caused by global warming.

The present study revealed an increasing trend in TBI1 in the deserts arid zone of the basin. It was not changing in the eastern low-temperature region. However, TBI2 revealed a significant rise in the cold eastern region. This indicates an increase in both Tmx and Tmn in arid desert zones in the center and west of ADRB. The increase in Tmn was much higher than the Tmn in the cold eastern region. Therefore, the increase in TBI2 was significant only in the cold eastern region. The results agree with the earlier studies conducted by (You et al., 2011) in China, (Araghi et al., 2016) in Iran and (Khan et al., 2019) in Pakistan. They showed a faster increase in TBI2 in the cold region than in the warm region. The results are also in harmony with the temperature changes in ADRB reported by (Wang et al., 2016). TBI3 showed a higher increase in temperature in cold months than in warmer months, which is significant in the cold region of the basin. This indicates the significant influence of TBI3 on critical thermal tolerance (Käfer et al., 2020). The trends in TBI4 collaborates with the results obtained by (Hadi Pour et al., 2019) in Iran. The TBI6 showed a significant increase over the west and central region of ADRB. An increase in temperature of the coldest month can be favourable for vegetation health and forest growth in the west and central region. The TBI7 showed significant change in a small patch in the south, and therefore, less implication in the basin.

6. Conclusion

The main objective of this study was the suitability assessment of gridded temperature datasets and the use of the best gridded temperature datasets to evaluate the trends in TBIs in ADRB. The CPI was used to rank the contradictory outcomes obtained by six statistical metrics in performance assessment of maximum and minimum temperature datasets to find the most

suitable dataset among selected products. Furthermore, the MCGDM method was employed to integrate the CPI of all stations to get a homogeneous result. The present study's finding indicates CPC as the most suitable gridded dataset in replicating in-situ temperature datasets over the ADRB. The study realized that CP could select the best temperature dataset in the basin as its result was well-matched with those given by most statistical indices. Therefore, future studies are highly recommended to use CPC for temperature trend analysis. The use of CPC of TBI trend analysis revealed a rise in average temperature in the basin in the range of 0.1 – 0.3℃/decade. The significant changes in TBI2 and TBI3 in the basin's east were due to the faster rise in Tmn than the Tmx. The highest increase was noticed for TBI6 compared to other indicators. It indicates an increase in Tmx in the warmest month was more pronounced over the basin, except in a small part in the east. In the future, other reanalysis and remote sensing temperature datasets can be compared to evaluate their performance in the basin. Other recently developed algorithms, particularly machine learning algorithms, can be employed to evaluate the ability of gridded data. The reliability of daily gridded temperature data to replicate the temperature extremes in the basin can also be evaluated in the future.

Acknowledgement

Author(s) are grateful to Universiti Teknologi Malaysia (UTM) for providing support to this research through grant no. Q.J130000.2451.09G07. The first author is grateful to the Ministry of Education of Afghanistan for providing fund to conduct this study. The authors are also thankful to the Ministry of Energy and Water of Afghanistan (MEW–AFG) and the National Oceanic and Atmospheric Administration (NOAA), the United States, for providing the data through their web portal to conduct this study.

Declarations

Funding

Author(s) are grateful to Universiti Teknologi Malaysia (UTM) for providing support to this research through grant no. Q.J130000.2451.09G07

Conflict of interest

The authors declare no conflict of interest.

Availability of data:

All the data are available in the public domain at the links provided in the texts

Code availability

The codes used for the processing of data can be provided on request to the corresponding author.

Authors' contribution

All the authors contributed to the conceptualization and design phases of the study. The data were gathered by Obaidullah Salehie and Saad Sh Sammen; the programming code was written by Shamsuddin Shahid and Anurag Malik; an initial draft of the paper was prepared by Obaidullah Salehie and Saad Sh Sammen; individual revisions and the final version were provided by Tarmizi bin Ismail and Xiaojun Wang.

References

Abatzoglou, J. T., Dobrowski, S. Z., Parks, S. A., and Hegewisch, K. C. (2018). TerraClimate, a high-resolution global dataset of monthly climate and climatic water balance from 1958–2015. Scientific data, 5(1), 1-12.

Adhikari, P., Shin, M.-S., Jeon, J.-Y., Kim, H. W., Hong, S., and Seo, C. (2018). Potential impact of climate change on the species richness of subalpine plant species in the mountain national parks of South Korea. Journal of Ecology and Environment, 42(1), 1-10.

Ahmed, K., Shahid, S., Wang, X., Nawaz, N., and Khan, N. (2019). Evaluation of gridded precipitation datasets over arid regions of Pakistan. Water, 11(2), 210.

Ancillotto, L., Santini, L., Ranc, N., Maiorano, L., and Russo, D. (2016). Extraordinary range expansion in a common bat: the potential roles of climate change and urbanization. The Science of Nature, 103(3-4), 15.

Araghi, A., Mousavi-Baygi, M., and Adamowski, J. (2016). Detection of trends in days with extreme temperatures in Iran from 1961 to 2010. Theoretical and Applied Climatology, 125(1), 213-225.

Attorre, F., Alfo', M., De Sanctis, M., Francesconi, F., and Bruno, F. (2007). Comparison of interpolation methods for mapping climatic and bioclimatic variables at regional scale. International Journal of Climatology: A Journal of the Royal Meteorological Society, 27(13), 1825-1843.

Bai, L., Shi, C., Li, L., Yang, Y., and Wu, J. (2018). Accuracy of CHIRPS satellite-rainfall products over mainland China. Remote Sensing, 10(3), 362.

Bashir, M. F., Ma, B., Komal, B., Bashir, M. A., Tan, D., and Bashir, M. (2020). Correlation between climate indicators and COVID-19 pandemic in New York, USA. Science of The Total Environment, 728, 138835.

Behar, O., Khellaf, A., and Mohammedi, K. (2015). Comparison of solar radiation models and their validation under Algerian climate–The case of direct irradiance. Energy Conversion and Management, 98, 236-251.

Błażejczyk, K. (2011). Assessment of regional bioclimatic contrasts in Poland. Miscellanea Geographica, 15(1), 79-91.

Brahim, H. B., and Duckstein, L. (2011). Descriptive methods and compromise programming for promoting agricultural reuse of treated wastewater Computational Methods for Agricultural Research: Advances and Applications (pp. 355-388): IGI Global.

Caesar, J., Alexander, L., and Vose, R. (2006). Large-scale changes in observed daily maximum and minimum temperatures: Creation and analysis of a new gridded data set. Journal of Geophysical Research: Atmospheres, 111(D5).

Cheng, J., Xu, Z., Zhu, R., Wang, X., Jin, L., Song, J., and Su, H. (2014). Impact of diurnal temperature range on human health: a systematic review. International journal of biometeorology, 58(9), 2011-2024.

Colston, J. M., Ahmed, T., Mahopo, C., Kang, G., Kosek, M., de Sousa Junior, F., . . . Zaitchik, B. (2018). Evaluating meteorological data from weather stations, and from satellites and global models for a multi-site epidemiological study. Environmental research, 165, 91-109.

Daemei, A. B., Eghbali, S. R., and Khotbehsara, E. M. (2019). Bioclimatic design strategies: A guideline to enhance human thermal comfort in Cfa climate zones. Journal of Building Engineering, 25, 100758.

Dakhil, M. A., Xiong, Q., Farahat, E. A., Zhang, L., Pan, K., Pandey, B., . . . Zhang, A. (2019). Past and future climatic indicators for distribution patterns and conservation planning of temperate coniferous forests in southwestern China. Ecological Indicators, 107, 105559.

Despotovic, M., Nedic, V., Despotovic, D., and Cvetanovic, S. (2015). Review and statistical analysis of different global solar radiation sunshine models. Renewable and Sustainable Energy Reviews, 52, 1869-1880.

Distler, T., Schuetz, J. G., Velásquez-Tibatá, J., and Langham, G. M. (2015). Stacked species distribution models and macroecological models provide congruent projections of avian species richness under climate change. Journal of Biogeography, 42(5), 976-988.

Evans, B. J., and Lyons, T. (2013). Bioclimatic extremes drive forest mortality in southwest, Western Australia. Climate, 1(2), 28-52.

Fan, J., Wang, X., Wu, L., Zhang, F., Bai, H., Lu, X., and Xiang, Y. (2018). New combined models for estimating daily global solar radiation based on sunshine duration in humid regions: a case study in South China. Energy Conversion and Management, 156, 618-625.

Fraga, H., Guimarães, N., and Santos, J. A. (2019). Future Changes in rice bioclimatic growing conditions in Portugal. Agronomy, 9(11), 674.

Gaitani, N., Mihalakakou, G., and Santamouris, M. (2007). On the use of bioclimatic architecture principles in order to improve thermal comfort conditions in outdoor spaces. Building and Environment, 42(1), 317-324.

Gampe, D., and Ludwig, R. (2017). Evaluation of gridded precipitation data products for hydrological applications in complex topography. Hydrology, 4(4), 53.

Gan, J., Colletti, J. P., and Kolison Jr, S. H. (1996). A compromise programming approach to integrated natural resource management. Paper presented at the Society of American foresters.

Gaybullaev, B., and Chen, S.-C. (2013). Water salinity changes of the gauging stations along the Amu Darya River. Journal of Agriculture and Forestry, 62(1), 1-14.

Guo, B., Zhang, J., Meng, X., Xu, T., and Song, Y. (2020). Long-term spatio-temporal precipitation variations in China with precipitation surface interpolated by ANUSPLIN. Scientific reports, 10(1), 1-17.

Haag, I., Jones, P. D., and Samimi, C. (2019). Central Asia's changing climate: How temperature and precipitation have changed across time, space, and altitude. Climate, 7(10), 123.

Hadi Pour, S., Abd Wahab, A. K., Shahid, S., and Wang, X. (2019). Spatial pattern of the unidirectional trends in thermal bioclimatic indicators in Iran. Sustainability, 11(8), 2287.

Hamasha, H., Schmidt-Lebuhn, A., Durka, W., Schleuning, M., and Hensen, I. (2013). Bioclimatic regions influence genetic structure of four Jordanian Stipa species. Plant Biology, 15(5), 882-891.

Hamed, K. H. (2008). Trend detection in hydrologic data: the Mann–Kendall trend test under the scaling hypothesis. Journal of Hydrology, 349(3-4), 350-363.

He, B., Huang, L., and Wang, Q. (2015). Precipitation deficits increase high diurnal temperature range extremes. Scientific Reports, 5(1), 1-7.

Hradilová, I., Duchoslav, M., Brus, J., Pechanec, V., Hýbl, M., Kopecký, P., . . . Bariotakis, M. (2019). Variation in wild pea (Pisum sativum subsp. elatius) seed dormancy and its relationship to the environment and seed coat traits. PeerJ, 7, e6263.

Islam, A. R. M. T., Islam, H. T., Shahid, S., Khatun, M. K., Ali, M. M., Rahman, M. S., . . . Almoajel, A. M. (2021). Spatiotemporal nexus between vegetation change and extreme climatic indices and their possible causes of change. Journal of Environmental Management, 289, 112505.

Jalilov, S.-M., Amer, S. A., and Ward, F. A. (2013). Reducing conflict in development and allocation of transboundary rivers. Eurasian Geography and Economics, 54(1), 78-109.

Jalilov, S.-M., Keskinen, M., Varis, O., Amer, S., and Ward, F. A. (2016). Managing the water–energy–food nexus: Gains and losses from new water development in Amu Darya River Basin. Journal of Hydrology, 539, 648-661.

Jamil, B., Irshad, K., Algahtani, A., Islam, S., Ali, M. A., and Shahab, A. (2020). On the calibration and applicability of global solar radiation models based on temperature extremities in India. Environmental Progress & Sustainable Energy, 39(1), 13236.

Käfer, H., Kovac, H., Simov, N., Battisti, A., Erregger, B., Schmidt, A. K., and Stabentheiner, A. (2020). Temperature tolerance and thermal environment of European seed bugs. Insects, 11(3), 197.

Kendall, M. (1975). Rank correlation methods. 2nd impression. Charles Griffin and Company Ltd. London and High Wycombe.

Khan, N., Shahid, S., bin Ismail, T., and Wang, X.-J. (2019). Spatial distribution of unidirectional trends in temperature and temperature extremes in Pakistan. Theoretical and Applied Climatology, 136(3), 899-913.

Khan, N., Shahid, S., Ismail, T., Ahmed, K., & Nawaz, N. (2019). Trends in heat wave related indices in Pakistan. Stochastic environmental research and risk assessment, 33(1), 287-302.

Khaydarov, M., and Gerlitz, L. (2019). Climate variability and change over Uzbekistan–an analysis based on high resolution CHELSA data. Central Asian Journal of Water Research (CAJWR) Центральноазиатский журнал исследований водных ресурсов, 5(2), 1-19.

Kim, Y., Park, C., Koo, K. A., Lee, M. K., and Lee, D. K. (2019). Evaluating multiple bioclimatic risks using Bayesian belief network to support urban tree management under climate change. Urban Forestry & Urban Greening, 43, 126354.

Koo, K. A., Kong, W.-S., Nibbelink, N. P., Hopkinson, C. S., and Lee, J. H. (2015). Potential effects of climate change on the distribution of cold-tolerant evergreen broadleaved woody plants in the Korean Peninsula. PloS one, 10(8), e0134043.

Kumar, N., Khamzina, A., Tischbein, B., Knöfel, P., Conrad, C., and Lamers, J. P. (2019). Spatio-temporal supply–demand of surface water for agroforestry planning in saline landscape of the lower Amudarya Basin. Journal of Arid Environments, 162, 53-61.

Li, W.-j., Peng, M.-c., Higa, M., Tanaka, N., Matsui, T., Tang, C. Q., . . . Yan, H.-z. (2016). Effects of climate change on potential habitats of the cold temperate coniferous forest in Yunnan province, southwestern China. Journal of Mountain Science, 13(8), 1411-1422.

Lutz, A. F., Immerzeel, W. W., Gobiet, A., Pellicciotti, F., and Bierkens, M. F. (2013). Comparison of climate change signals in CMIP3 and CMIP5 multi-model ensembles and implications for Central Asian glaciers. Hydrology and Earth System Sciences, 17(9), 3661-3677.

Ma, Q., Wu, J., and He, C. (2016). A hierarchical analysis of the relationship between urban impervious surfaces and land surface temperatures: spatial scale dependence, temporal variations, and bioclimatic modulation. Landscape Ecology, 31(5), 1139-1153.

Mahmood, R., Jia, S., and Zhu, W. (2019). Analysis of climate variability, trends, and prediction in the most active parts of the Lake Chad basin, Africa. Scientific reports, 9(1), 1-18.

Mancinelli, G., Mali, S., and Belmonte, G. (2019). Species richness and taxonomic distinctness of zooplankton in ponds and small lakes from Albania and North Macedonia: the role of bioclimatic factors. Water, 11(11), 2384.

Mann, H. B. (1945). Nonparametric tests against trend. Econometrica: Journal of the econometric society, 245-259.

Meseguer-Ruiz, O., Ponce-Philimon, P. I., Quispe-Jofré, A. S., Guijarro, J. A., & Sarricolea, P. (2018). Spatial behaviour of daily observed extreme temperatures in Northern Chile (1966–2015): data quality, warming trends, and its orographic and latitudinal effects. Stochastic Environmental Research and Risk Assessment, 32(12), 3503-3523.

Miguet, F., and Groleau, D. (2007). Urban bioclimatic indicators for urban planners with the software tool SOLENE. Portugal SB07 Sustainable Construction, materials and practices: challenges of the industry for the new millennium, Lisbon, Portugal, 348-355.

Monterroso, P., Alves, P. C., and Ferreras, P. (2014). Plasticity in circadian activity patterns of mesocarnivores in Southwestern Europe: implications for species coexistence. Behavioral Ecology and Sociobiology, 68(9), 1403-1417.

Moriondo, M., Trombi, G., Ferrise, R., Brandani, G., Dibari, C., Ammann, C. M., . . . Bindi, M. (2013). Olive trees as bio-indicators of climate evolution in the M editerranean B asin. Global Ecology and Biogeography, 22(7), 818-833.

Muhammad, M. K. I., Nashwan, M. S., Shahid, S., Ismail, T. b., Song, Y. H., and Chung, E.-S. (2019). Evaluation of empirical reference evapotranspiration models using compromise programming: a case study of Peninsular Malaysia. Sustainability, 11(16), 4267.

Musie, M., Sen, S., and Srivastava, P. (2019). Comparison and evaluation of gridded precipitation datasets for streamflow simulation in data scarce watersheds of Ethiopia. Journal of hydrology, 579, 124168.

Nashwan, M. S., and Shahid, S. (2019). Symmetrical uncertainty and random forest for the evaluation of gridded precipitation and temperature data. Atmospheric Research, 230, 104632.

Nashwan, M. S., Shahid, S., and Abd Rahim, N. (2019). Unidirectional trends in annual and seasonal climate and extremes in Egypt. Theoretical and Applied Climatology, 136(1), 457-473.

Nashwan, M. S., Shahid, S., and Wang, X. (2019). Uncertainty in estimated trends using gridded rainfall data: a case study of Bangladesh. Water, 11(2), 349.

New, M., Hulme, M., and Jones, P. (2000). Representing twentieth-century space–time climate variability. Part II: Development of 1901–96 monthly grids of terrestrial surface climate. Journal of Climate, 13(13), 2217-2238.

Newman, A. J., Clark, M. P., Craig, J., Nijssen, B., Wood, A., Gutmann, E., . . . Arnold, J. R. (2015). Gridded ensemble precipitation and temperature estimates for the contiguous United States. Journal of Hydrometeorology, 16(6), 2481-2500.

Nezlin, N. P., Kostianoy, A. G., and Lebedev, S. A. (2004). Interannual variations of the discharge of Amu Darya and Syr Darya estimated from global atmospheric precipitation. Journal of marine systems, 47(1-4), 67-75.

Nijssen, B., and Lettenmaier, D. P. (2004). Effect of precipitation sampling error on simulated hydrological fluxes and states: Anticipating the Global Precipitation Measurement satellites. Journal of Geophysical Research: Atmospheres, 109(D2).

Nix, H. A. (1986). A biogeographic analysis of Australian elapid snakes. Atlas of elapid snakes of Australia, 7, 4-15.

Noce, S., Caporaso, L., and Santini, M. (2020). A new global dataset of bioclimatic indicators. Scientific data, 7(1), 1-12.

O'Donnell, M. S., and Ignizio, D. A. (2012). Bioclimatic predictors for supporting ecological applications in the conterminous United States. US Geological Survey Data Series, 691(10), 4-9.

Pour, S. H., Abd Wahab, A. K., and Shahid, S. (2020). Spatiotemporal changes in precipitation indicators related to bioclimate in Iran. Theoretical and Applied Climatology, 141(1), 99-115.

Rai, S., Sharma, S., Shrestha, K., Gajurel, J., Devkota, S., Nobis, M., and Scheidegger, C. (2016). Effects of the environment on species richness and composition of vascular plants in Manaslu Conservation Area and Sagarmatha region of Nepalese Himalaya. Banko Janakari, 26(1), 3-16.

Raju, K. S., Sonali, P., and Kumar, D. N. (2017). Ranking of CMIP5-based global climate models for India using compromise programming. Theoretical and Applied Climatology, 128(3-4), 563-574.

Reitalu, T., Helm, A., Pärtel, M., Bengtsson, K., Gerhold, P., Rosén, E., . . . Prentice, H. C. (2014). Determinants of fine-scale plant diversity in dry calcareous grasslands within the Baltic Sea region. Agriculture, ecosystems & environment, 182, 59-68.

Saddique, N., Khaliq, A., & Bernhofer, C. (2020). Trends in temperature and precipitation extremes in historical (1961–1990) and projected (2061–2090) periods in a data scarce mountain basin, northern Pakistan. Stochastic Environmental Research and Risk Assessment, 34(10), 1441-1455.

Sajani, S. Z., Tibaldi, S., Scotto, F., and Lauriola, P. (2008). Bioclimatic characterization of an urban area: a case study in Bologna (Italy). International journal of biometeorology, 52(8), 779-785.

Salat, S. (2007). Energy and bioclimatic efficiency of urban morphologies: towards a comparative analysis of Asian and European cities. Paper presented at the Proceedings of the International Conference on Sustainable Building Asia.

Salman, S. A., Shahid, S., Ismail, T., Ahmed, K., and Wang, X.-J. (2018). Selection of climate models for projection of spatiotemporal changes in temperature of Iraq with uncertainties. Atmospheric Research, 213, 509-522.

Salman, S. A., Shahid, S., Ismail, T., Al-Abadi, A. M., Wang, X.-j., and Chung, E.-S. (2019). Selection of gridded precipitation data for Iraq using compromise programming. Measurement, 132, 87-98.

Savoskul, O., and Shevnina, E. (2015). Irrigated crop production in the Syr Darya Basin: climate change rehearsal in the 1990s. Climate Change and Agricultural Water Management in Developing Countries, 8, 176.

Schlüter, M., Savitsky, A. G., McKinney, D. C., and Lieth, H. (2005). Optimizing long-term water allocation in the Amudarya River delta: a water management model for ecological impact assessment. Environmental Modelling & Software, 20(5), 529-545.

Schröder, W., Schmidt, G., and Schönrock, S. (2014). Modelling and mapping of plant phenological stages as bio-meteorological indicators for climate change. Environmental Sciences Europe, 26(1), 1-13.

Sen, P. K. (1968). Estimates of the regression coefficient based on Kendall's tau. Journal of the American statistical association, 63(324), 1379-1389.

Shahid, S., Harun, S. B., and Katimon, A. (2012). Changes in diurnal temperature range in Bangladesh during the time period 1961–2008. Atmospheric Research, 118, 260-270.

Sheffield, J., Goteti, G., and Wood, E. F. (2006). Development of a 50-year high-resolution global dataset of meteorological forcings for land surface modeling. Journal of Climate, 19(13), 3088-3111.

Shibuo, Y., Jarsjö, J., and Destouni, G. (2007). Hydrological responses to climate change and irrigation in the Aral Sea drainage basin. Geophysical Research Letters, 34(21).

Sidike, A., Chen, X., Liu, T., Durdiev, K., and Huang, Y. (2016). Investigating alternative climate data sources for hydrological simulations in the upstream of the Amu Darya River. Water, 8(10), 441.

Sommer, J. H., Kreft, H., Kier, G., Jetz, W., Mutke, J., and Barthlott, W. (2010). Projected impacts of climate change on regional capacities for global plant species richness. Proceedings of the Royal Society B: Biological Sciences, 277(1692), 2271-2280.

Sosa, V., and Loera, I. (2017). Influence of current climate, historical climate stability and topography on species richness and endemism in Mesoamerican geophyte plants. PeerJ, 5, e3932.

Sun, J., Li, Y., Suo, C., and Liu, Y. (2019). Impacts of irrigation efficiency on agricultural water-land nexus system management under multiple uncertainties—A case study in Amu Darya River basin, Central Asia. Agricultural Water Management, 216, 76-88.

Tanarhte, M., Hadjinicolaou, P., and Lelieveld, J. (2012). Intercomparison of temperature and precipitation data sets based on observations in the Mediterranean and the Middle East. Journal of Geophysical Research: Atmospheres, 117(D12).

Törnqvist, R. (2013). Basin-scale change in water availability and water quality under intensified irrigated agriculture. Department of Physical Geography and Quaternary Geology, Stockholm University.

Wang, S., Xu, X., Shrestha, N., Zimmermann, N. E., Tang, Z., and Wang, Z. (2017). Response of spatial vegetation distribution in China to climate changes since the Last Glacial Maximum (LGM). PloS one, 12(4), e0175742.

Wang, X., Luo, Y., Sun, L., He, C., Zhang, Y., and Liu, S. (2016). Attribution of runoff decline in the Amu Darya River in Central Asia during 1951–2007. Journal of Hydrometeorology, 17(5), 1543-1560.

White, C. J., Tanton, T. W., and Rycroft, D. W. (2014). The impact of climate change on the water resources of the Amu Darya Basin in Central Asia. Water Resources Management, 28(15), 5267-5281.

Xie, P., Chen, M., and Shi, W. (2010). CPC unified gauge-based analysis of global daily precipitation. Paper presented at the Preprints, 24th Conf. on Hydrology, Atlanta, GA, Amer. Meteor. Soc.

Xu, H., Xu, C. Y., Sælthun, N. R., Zhou, B., & Xu, Y. (2015). Evaluation of reanalysis and satellite-based precipitation datasets in driving hydrological models in a humid region of Southern China. Stochastic Environmental Research and Risk Assessment, 29(8), 2003-2020.

Yaro, C. A., Kogi, E., Luka, S. A., Nassan, M. A., Kabir, J., Opara, K. N., . . . Batiha, G. E.-S. (2021). Edaphic and climatic factors influence on the distribution of soil transmitted helminths in Kogi East, Nigeria. Scientific Reports, 11(1), 1-12.

Yasutomi, N., Hamada, A., and Yatagai, A. (2011). Development of a long-term daily gridded temperature dataset and its application to rain/snow discrimination of daily precipitation. Global Environmental Research, 15(2), 165-172.

Yin, H., Donat, M. G., Alexander, L. V., and Sun, Y. (2015). Multi-dataset comparison of gridded observed temperature and precipitation extremes over China. International Journal of Climatology, 35(10), 2809-2827.

You, Q., Kang, S., Aguilar, E., Pepin, N., Flügel, W.-A., Yan, Y., . . . Huang, J. (2011). Changes in daily climate extremes in China and their connection to the large scale atmospheric circulation during 1961–2003. Climate Dynamics, 36(11-12), 2399-2417.

Zeleny, M. (1973). Compromise programming. Multiple criteria decision making.

Zhang, J., Zhou, Y., Zhou, G., and Xiao, C. (2013). Structure and composition of natural Gmelin larch (Larix gmelinii var. gmelinii) forests in response to spatial climatic changes. PloS one, 8(6), e66668.

Zhang, W. (2003). A compromise programming method using multibounds formulation and dual approach for multicriteria structural optimization. International journal for numerical methods in engineering, 58(4), 661-678.

Supplementary Materials

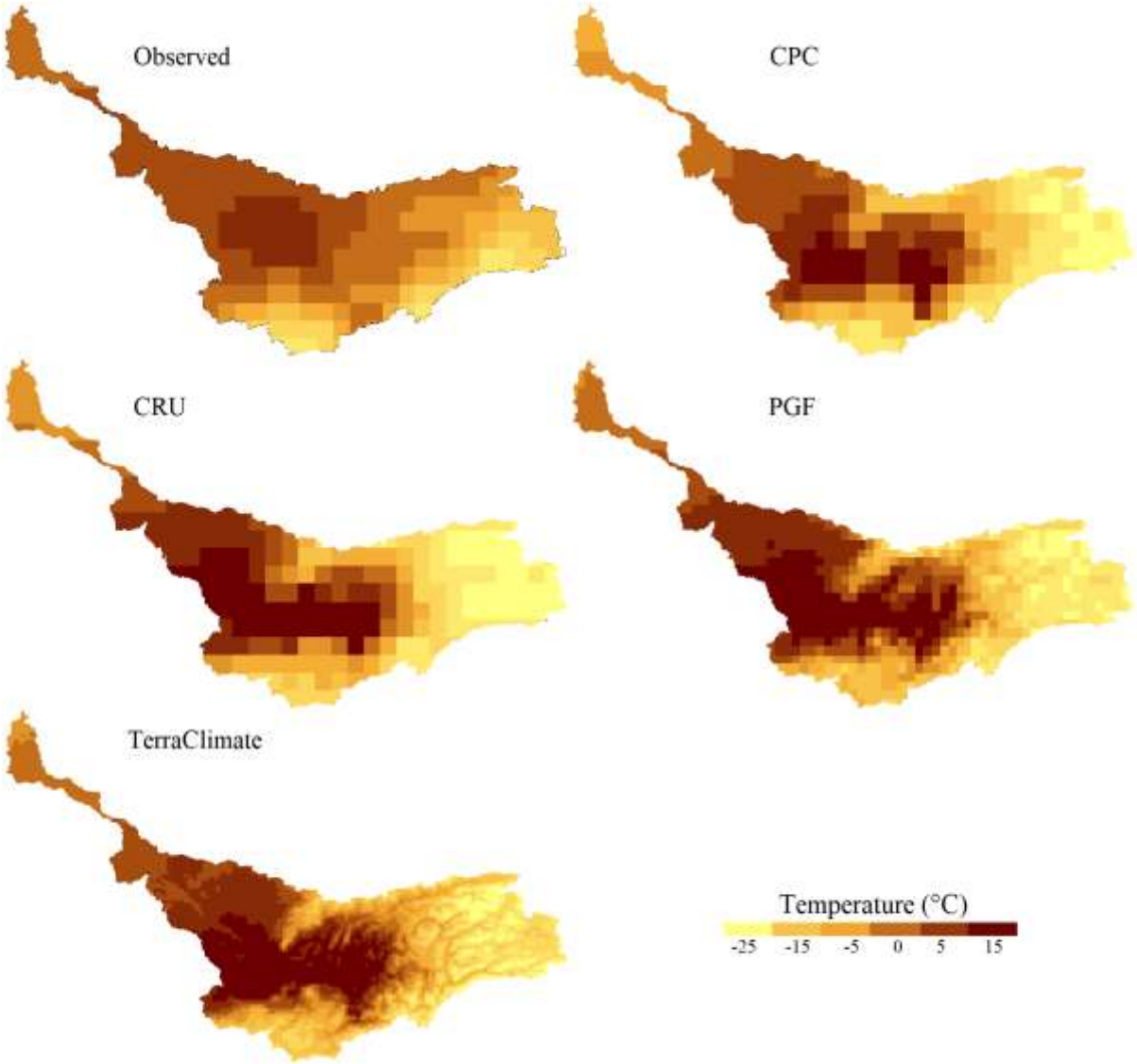

Figure S-1. Average daily minimum temperature estimated by different gridded datasets over the basin for the periods they were available.

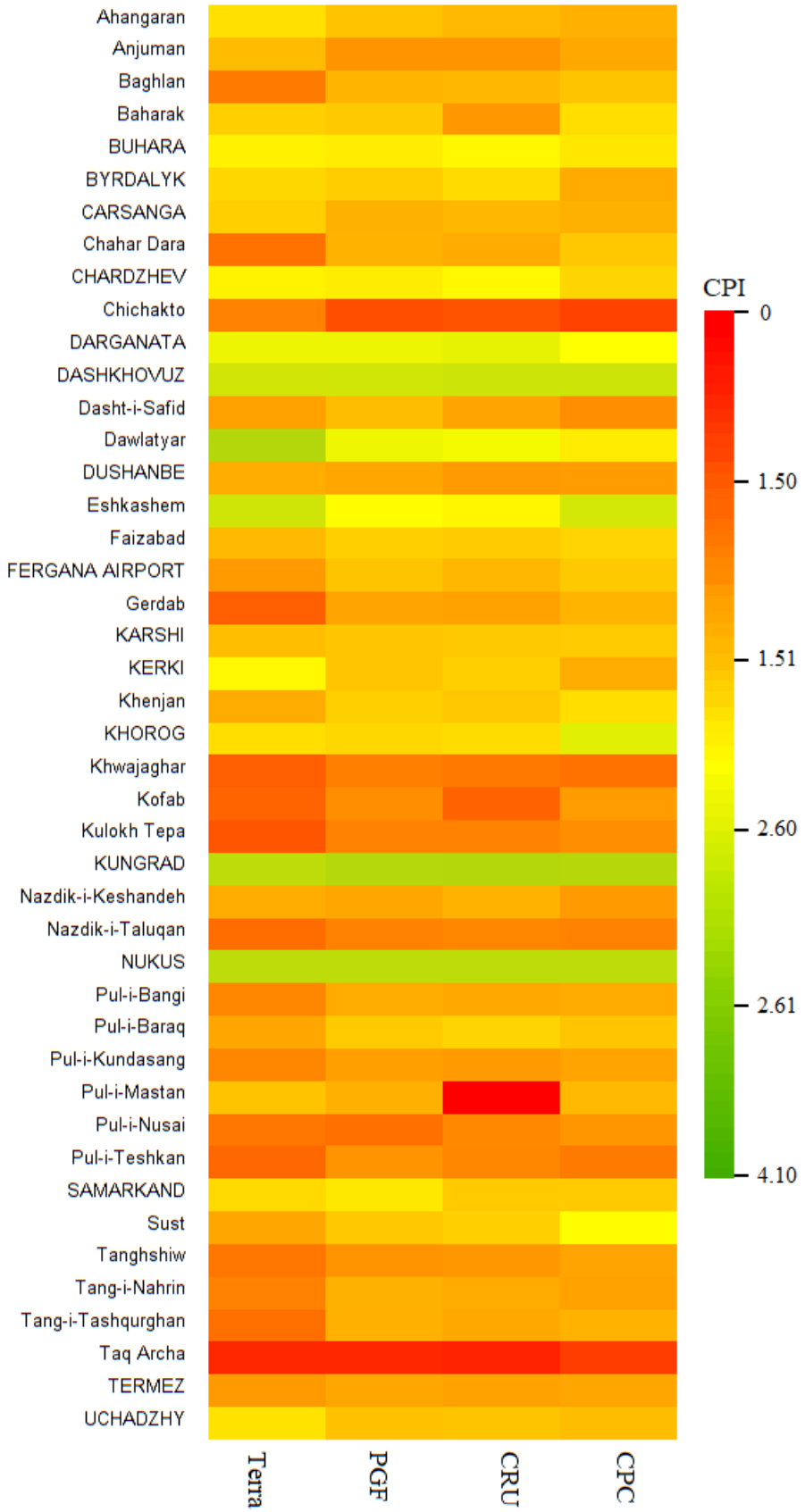

Figure S-2. Heatmap of CPI for all gridded minimum temperature datasets used in this study